ADVANCED FUNCTIONAL MATERIALS
www.afm-journal.de

Surface-Confined Heterometallic Molecular Dyads: Merging the Optical and Electronic Properties of Fe, Ru, and Os Terpyridyl Complexes

Tarkeshwar Gupta, Prakash Chandra Mondal, Anup Kumar, Yekkoni Lakshmanan Jeyachandran, and Michael Zharnikov**

Molecular assemblies of surface-confined heterometallic molecular dyads (SURHMDs) composed of optically rich and redox-active $Fe(pytpy)_2{\cdot}2PF_6$ (Fe-PT), $Ru(pytpy)_2{\cdot}2PF_6$ (Ru-PT) and $Os(pytpy)_2{\cdot}2PF_6$ (Os-PT) pytpy = 4′-(4-pyridyl)-2,2′:6′,2″-terpyridyl] complexes are fabricated via bottom-up approach on SiO_x based solid supports. Pairing of the two different metal-organic complexes at a single platform results in significant enlargement of the optical window (λ = 400–800 nm), which can be of interest for potential applications. The use of the Cu-based linker ensures intramolecular electronic communication between these complexes. In addition, SURHMDs are electrochemically stable under large numbers of read-write cycles (10^3) and exhibit multiple redox states at relatively low potentials (<1.2 V). Moreover, an electrochemical input at controlled potentials creates a mixed-valence multicomponent system.

1. Introduction

Surface-confined inorganic-organic hybrid materials[1] provide a promising platform to integrate smart optical and electronic components for the development of novel architectures that are capable of rapid processing of information and multibit storage.[2] Consequently, a variety of bottom-up and top-down approaches such as fabrication of monolayers, multilayers and patterned layers or lithographic strategies have been developed to construct such materials.[3] To date, however, the critical question of whether these molecular-based assemblies can meet the standards of electronic devices such as large and multiple charge retention, durability, stability, and remote accessibility still needs to be addressed.[2]

Prof. T. Gupta, P. C. Mondal, A. Kumar
Department of Chemistry
University of Delhi
Delhi 110007, India
E-mail: tgupta@chemistry.du.ac.in
Dr. Y. L. Jeyachandran, Prof. M. Zharnikov
Lehrstuhl für Angewandte Physikalische Chemie
Universität Heidelberg
Heidelberg, 69120, Germany
E-mail: michael.zharnikov@urz.uni-heidelberg.de

DOI: 10.1002/adfm.201203404

Most recent state-of-the-art approaches entail the development of hybrid semiconductor/redox-active molecular materials wherein the information can be stored in the discrete redox states of the molecules. For instance, a broad design flexibility of porphyrins has been exploited by Lindsey, Bocian and others to assemble a variety of functional monolayer and multilayer systems that are capable to store charge on silicon-based solid supports.[2a,2c,4] Alternatively, polypyridyl complex based materials are emerging as an attractive platform to fabricate molecular-based memory elements and communication devices. The high temporal, thermal, and photochemical stability, extraordinary electrochemical characteristics such as redox reversibility, low writing and erasing voltages, fast electron transfer rate, and charge holding capability for extended period (up to hours) make these materials suitable candidates for charge-based data storage elements.[3e,5] In this context, homonuclear polypyridyl complex based monolayers and multilayers on metallic or insulating substrates have been prepared and extensively explored.[2d,3c,5d,6] However, to date, a little attention (with few exceptions)[6e,7] has been paid to the fabrication of heteronuclear polypyridyl complex based systems, even though they have lot of advantages as compared to the homonuclear constructs.[3a,6a,7b,8] In particular, assemblies of more than one type of redox-active components or coupling of heterometallic segments offer multiple redox centers that can mediate multibit charge-based data storage at molecular level. Equally important is to enlarge the optical window (into visible region) of the surface-confined materials. Additionally, use of semiconductor substrates such as ITO or doped Si and utilization of highly conducting metals such as copper as a linker provide substantial advantages in terms of molecular electronics.

In view of these fascinating aspects, we report herein on i) coordination-based assembly of heterogeneous dyads comprised of the terpyridyl-based metallo-organic complexes bridged via Cu^{2+} linker on Si, glass, and indium-tin-oxide (ITO) coated glass substrates, and ii) preliminary results regarding merged/enhanced optical properties of these systems and electronic communication between the metal centers of the complexes and the underlying substrate. As building blocks of the

heterogeneous dyads, we used well-known,[3a,9] optically-rich and redox-active $Fe(pytpy)_2 \cdot 2PF_6$ (Fe-PT), $Ru(pytpy)_2 \cdot 2PF_6$ (Ru-PT) and $Os(pytpy)_2 \cdot 2PF_6$ (Os-PT) [pytpy = 4′-(4-pyridyl)-2,2′:6′,2″-terpyridyl] complexes (see Figure S1, Supporting Information), which are capable of covalent attachment on a variety of substrates. We will refer to these complexes as M-PT (vide infra), where M = Fe, Ru and Os, respectively. Note that functional terpyridyl ligands (e.g., 4′-pyridyl terpyridyl) and their derivatives offer several synthetic and structural advantages owing to their excellent structure-properties correlations. The reasons behind the selection of functionalized 2,2′:6′,2″-terpyridyl ligands in the present work are: i) their strong chelating effect towards the transition metal ions, ii) facile synthetic route, iii) versatile coordination modes, and iv) the π-electron accepting nature of the terpyridine derivatives tends to stabilize the metal ions in lower oxidation states.[5f]

We would like to stress that our methodology differs from the previous work related to immobilization of multi-redox species on solid supports, which include either mixed SAM approach[4c] or confinement of heteronuclear complexes linked via organic moieties.[7a,10] However, it was found that organic linker does not effectively promote the electronic communication between two metal centers.[7a,11] In this regard, moieties containing conducting metals (Cu in the given work) as a linker may probably act as a better messenger.

2. Results and Discussion

2.1. General Procedure

The fabrication of hetero-metallic molecular dyads on SiO_x-based substrates is schematically illustrated in **Scheme 1**; it was performed by stepwise metal-metalloligand coordination reaction; the details are given in Section 4. In the first step, a SiO_x-based substrate such as transparent glass (for optical studies), relatively smooth silicon/silicon oxide (for microscopic studies) or conducting indium tin oxide (ITO) coated glass (for electrochemical studies) was cleaned, activated, and functionalized by immersion in a dry *n*-pentane solution of 3-iodo-*n*-propyl-trimethoxy-silane. The resulting iodo-terminated coupling layer (CL) was used as a primary template to assemble a monolayer of Fe-PT, Ru-PT or Os-PT in the second step of the preparation procedure. These monolayers served as secondary (major) template for the further preparation steps (see below) but are

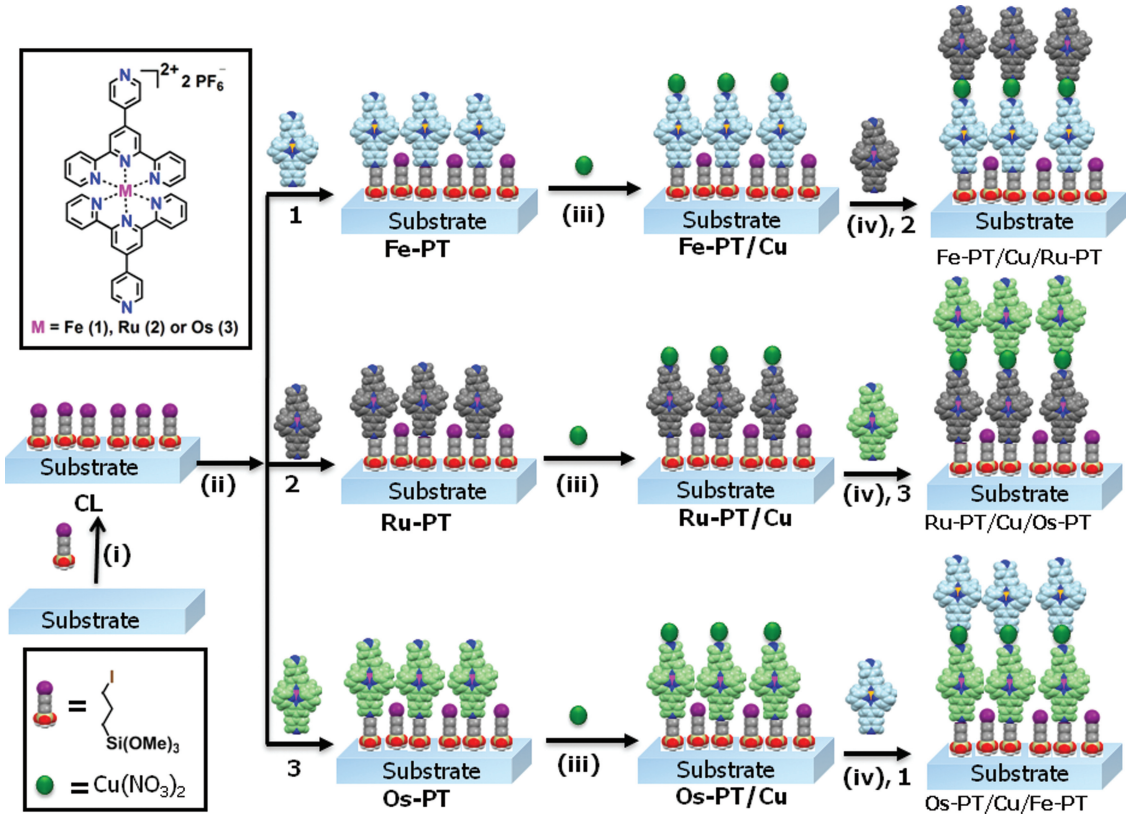

Scheme 1. Scheme for the fabrication of hetero-metallic molecular dyads on a solid support: i) immobilization of 3-iodo-*n*-propyl-trimethoxysilane on a SiOx substrate to form coupling layer (CL) serving as a primary template, ii) quaternization of the pendant pyridyl group of Fe-PT, Ru-PT or Os-PT to CL to form a secondary template layer, iii) coordination of copper nitrate with pyridine-terminated template layer to form Cu-terminated tertiary template layer, and iv) coordination of Ru-PT, Os-PT and Fe-PT with the Cu-terminated template layer to form the hetero-metallic molecular dyads. The counter anions (I^-, NO_3^-) or solvent molecules present in the lattice are omitted for clarity.

also of interest and practical importance on their own. In particular, they were found to be stable for months under dark and ambient conditions as judged by UV-vis spectroscopy. Neither washing with common solvent nor mechanical abrasion could remove the film. In addition, the Fe-PT, Ru-PT or Os-PT-based monolayers exhibited excellent thermal stability up to 200 °C as judged by UV-Vis spectroscopy at elevated temperatures (see Figure S2, Supporting Information), which is common for polypyridyl metal complex-based monolayers.[5b] Further, the template layers show good redox stability/reversibility and do not degrade upon large number of read-write cycles (10^3 times).

In the next step, the above robust secondary template layers were coordinated with $Cu(NO_3)_2$. Finally, the resulting films were used as tertiary templates for assembly of dissimilar Fe-PT, Ru-PT or Os-PT, resulting in hetero-metallic molecular dyads. Representative of different combinations of Fe-PT, Ru-PT or Os-PT, we fabricated Fe-PT/Cu/Ru-PT, Ru-PT/Cu/Os-PT, and Os-PT/Cu/Fe-PT dyads as shown in Scheme 1. Note that the above surface-supported, stepwise coordination reaction methodology is reliable, quite flexible and relatively simple as compared to synthesis and immobilization of a single molecule that exhibits multiple redox states or fabrication of a mixed SAM that bounces non-identical ratio of both components due to dissimilar reactivity. In addition, this methodology should also be suitable to extend the system to triads, tetrads, etc. in order to increase the number of redox states or stored bits.

2.2. Basic Characterization of the Template and Dyad Layers

The fabrication of hetero-metallic molecular dyads was monitored by a variety of complementary experimental techniques including atomic force microscopy (AFM), static contact angle (CA) goniometry, spectroscopic ellipsometry, X-ray photoelectron spectroscopy (XPS), and near-edge X-ray atomic fine structure (NEXAFS) spectroscopy.

The tapping-mode AFM images of the M-PT monolayers serving as the major template layer (see above) showed a relatively smooth film surface with no apparent features such as islands, grains, pinholes or defects (**Figure 1**a; for Fe-PT). Root-mean-square (RMS) roughness, R_{rms} measured for 1.5 μm × 1.5 μm scan areas was found to be ≈0.46 nm. The CA goniometry measurements showed a rather hydrophobic surface with aqueous CA values of around 76°. Similar values, varying from 74° to 83°, were obtained for the molecular dyad assemblies, which is reasonable since both M-PT and dyad films are terminated with relatively hydrophobic pyridine moiety. In contrast, Cu-terminated tertiary template layers such as Fe-PT/Cu exhibited lower values of CA (≈58°), as expected in view of the hydrophilicity of the copper ion. Ellipsometry-derived film thickness for representative template layer of Fe-PT was found to be ≈18.5 Å. Notably, the optimized length of Fe-PT including 3-iodo-*n*-propyltrimethoxy-silane is estimated at ≈24.1 Å, as determined by the Chem3D Pro energy minimization model, that is somewhat longer (≈5.6 Å) than the ellipsometry-derived thickness value. This shows that the Fe-PT is not standing strictly upright within the monolayer film but is somewhat tilted (≈30°) with respect to the surface normal (similar behavior can be expected for the Os-PT and Ru-PT films). The ellipsometry-derived thickness of the immobilized molecular dyads was found in a range of 25–32 Å implying a tilt of the second M-PT complex as well, owing to the square pyramidal geometry at the copper center.[12]

The intermediate templates and fabricated dyads were also characterized by XPS and NEXAFS spectroscopy. Representative of the entire family of the M_1-PT/Cu/M_2-PT dyads, we present here some selected data for the Os-PT template layer and Os-PT/Cu/Fe-PT dyad assembly on Si(100). XPS spectra of the Os-PT template layer exhibit characteristic Si 2p peaks from the substrate as well as C 1s, Os 4f, and N 1s emissions from the attached molecules. The Si 2p spectrum exhibits Si 2p doublets at 99.15 and 102.6 eV representative of non-oxidized and oxidized silicon, respectively. The relative intensity of the latter doublet increases with decreasing sampling depth of XPS suggesting that this is the surface of the substrate, which is oxidized. The N 1s spectrum exhibits an asymmetric peak which can be decomposed into two components at ≈399.7 and ≈402.0 eV (Figure 1b) related to the pyridine rings in the inner core of Os-PT (N) and pyridinium unit(s) (N^+) associated with the pendant pyridine rings. The respective intensity ratio, I(N)/I(N^+) = 6.7:1 indicates quaternization of only "bottom" (with respect to the substrate) pendent pyridine nitrogen which interacts with the coupling layer as sustained by the presumable orientation of the molecules. The Os 4f spectrum in Figure 1c shows Os $4f_{7/2,5/2}$ doublet at ≈50.5 eV ($4f_{7/2}$) with a characteristic branching ratio of 4:3 manifesting the expected presence of this metal ion. The C 1s spectrum (not shown) displays a somewhat asymmetric peak at 284.6 eV attributed to the pyridine moieties; the asymmetry is related to the binding energy shift between the carbon atoms in the meta, para, and ortho positions of the pyridine ring.[13]

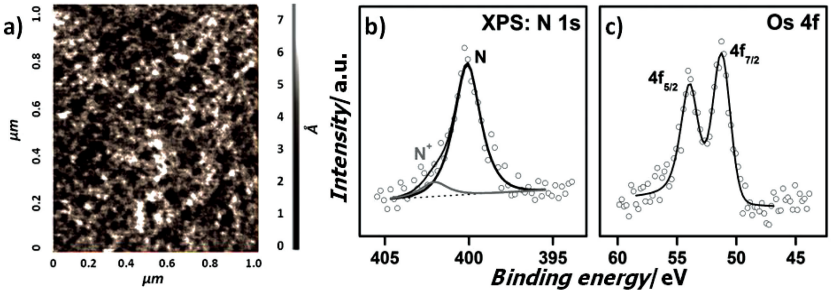

Figure 1. a) Representative AFM image of a M-PT template layer (Fe-PT in the given case) on Si(100); scan area 1.0 μm × 1.0 μm. b) N 1s and Os 4f XPS spectra of the Os-PT template layer on Si(100). The open circles represent the experimental data; the black solid lines the respective envelopes or fits. The N 1s spectrum is decomposed into two contributions assigned to the pyridine rings in the core of Os-PT and the "top" pendant pyridine moiety (N; black line) and to the "bottom" pendant pyridine ring bonded to the iodine-terminated CL (pyridinium unit, N^+, gray line).

The XPS spectra of Os-PT/Cu/Fe-PT on Si(100) are shown in **Figure 2**. The Si 2p spectrum in Figure 2a exhibits Si 2p doublets at 99.15 and 102.6 eV representative of the oxidized (topmost layers) silicon substrate.

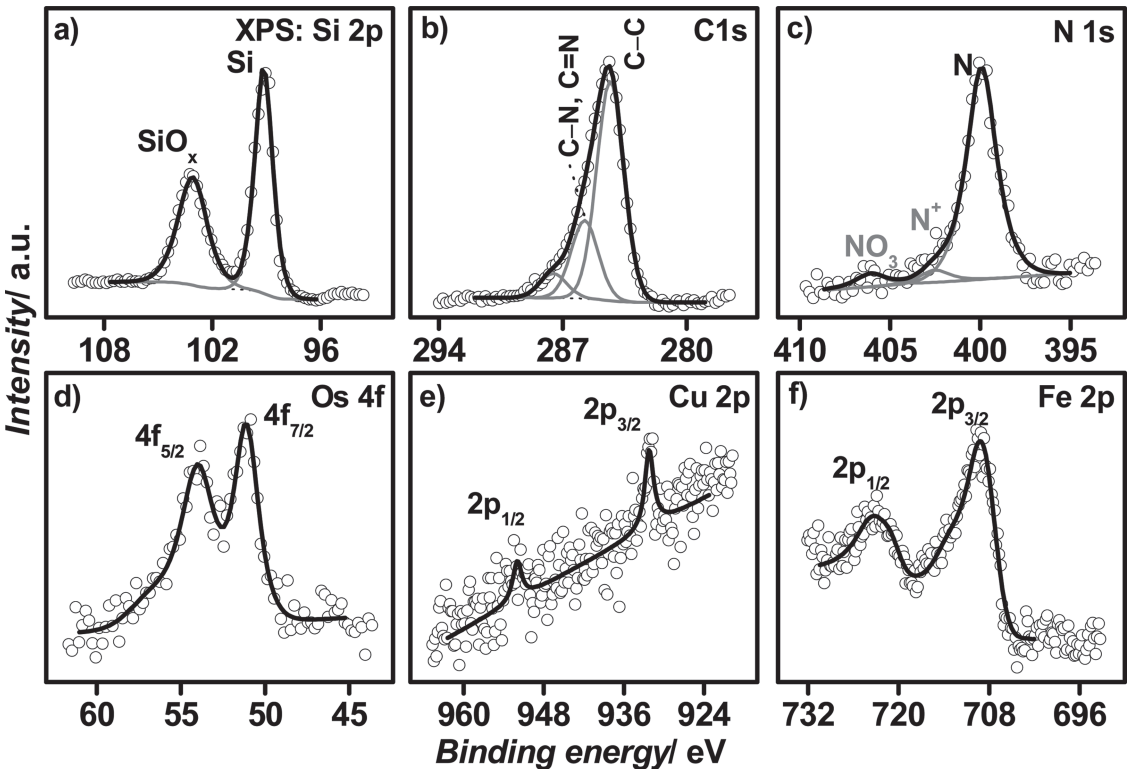

Figure 2. Si 2p (a), C 1s (b), N 1s (c), Os 4f (d), Cu 2p (e), and Fe 2p (f) XPS spectra of Os-PT/Cu/Fe-PT on Si(100). The open circles represent the experimental data; the black solid lines the respective envelopes or fits. The N 1s spectrum is decomposed into three components related to the pyridine rings in the core of Os-PT and Fe-PT as well as some of the pendant pyridine moieties (N; gray line), to the pendant pyridine ring bonded to the iodine-terminated primary template (pyridinium unit, N^+, gray line), and $Cu(NO_3)_2$ linker, respectively.

The C 1s spectrum in Figure 2b displays a somewhat asymmetric peak at 284.6 eV attributed to the pyridine moieties of Os-PT and Fe-PT; this peak is accompanied by a small feature at 287.5 eV assigned to a contamination (CO). The N 1s spectrum can be decomposed into three components related to the pyridine rings in the core of Os-PT and Fe-PT as well as to some of the pendant pyridine moieties (N), pyridine ring bonded to the iodine-terminated primary template (pyridinium unit, N^+), and $Cu(NO_3)_2$ linker, respectively (Figure 2c). The Os 4f, Cu 2p, and Fe 2p spectra in Figure 2d–f exhibit the characteristic signals manifesting the expected presence of the above metal ions in the Os-PT/Cu/Fe-PT dyad layer.

C K-edge and N K-edge NEXAFS spectra of Os-PT/Cu/Fe-PT on Si(100) are shown in **Figure 3**. These spectra were acquired at an X-ray incidence angle of 55° which excludes the influence of the orientation effects.[14] Both C and N K-edge spectra exhibit the characteristic resonance structure of pyridine, viz. a pronounced double 1π* resonance at 284.7 and 285.5 eV at the C K-edge and a strong π* resonance at 399.6 eV at the N K-edge.[15] Note that the splitting of the 1π* resonance at the C K-edge as compared to benzene, for which only a single 1π* resonance at ≈285.0 eV is observed,[15a] is related to the different C 1s core level binding energies for the carbon atoms in the ortho positions (C=N) and those in the meta and para positions (C=C) of the pyridine ring.[15b] Note also that the NEXAFS spectra of Os-PT/Cu/Fe-PT on Si(100) did not exhibit pronounced dependence of the absorption resonance intensity on the angle of X-ray incidence, so-called linear dichroism.[14] The lack of the linear dichroism is presumably related to the

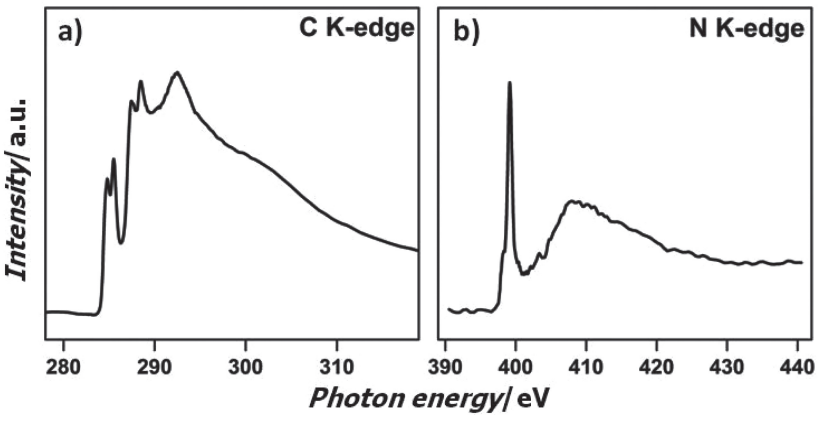

Figure 3. C K-edge (a) and N K-edge (b) NEXAFS spectra of Os-PT/Cu/Fe-PT on Si(100). The spectra were acquired at an X-ray incidence angle of 55°.

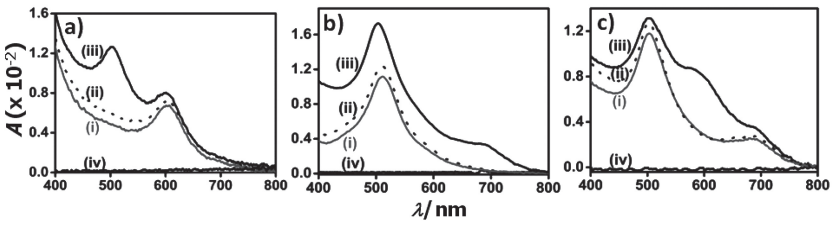

Figure 4. UV-vis absorption spectra of the secondary (gray lines) and tertiary (dotted black lines) template layers as well as resulting hetero-metallic molecular dyads (black lines) on glass substrates. a) Fe-PT (i), Fe-PT/Cu (ii), Fe-PT/Cu/Ru-PT (iii); b) Ru-PT (i), Ru-PT/Cu (ii), and Ru-PT/Cu/Os-PT (iii); c) Os-PT (i), Os-PT/Cu (ii), and Os-PT/Cu/Fe-PT (iii). (iv) represent the baselines.

specific coupling geometry of the pendant pyridine moieties and different torsions of individual pyridine rings within the assembled dyads.

2.3. Optical Properties

The fabrication of heterometallic molecular dyads on glass substrate was monitored by UV-vis spectroscopy. UV-Vis spectra of the Fe-PT, Ru-PT and Os-PT template layers on glass substrates exhibit a characteristic metal-to-ligand charge-transfer (MLCT) band at λ_{max} = 605, 511, and 502 nm respectively (**Figure 4**). This band is comparable to the analogous band of Fe-PT, Ru-PT and Os-PT in CH_3CN solution (see Figure S3, Supporting Information) with a red shift of $\Delta\lambda$ = +36, +21, and +12 nm, respectively. The above red shift is attributed to the quaternization of the "bottom" pendant pyridine group with the iodo-terminated coupling layer assembled on the substrate.[16] In addition, intermolecular interaction within the densely packed M-PT film could be another factor for the observed wavelength shift as compared to the solution where the molecules behave individually.[17a] From the UV-vis data, the average packing density of the Fe-PT, Ru-PT and Os-PT template layers on glass was estimated roughly at ≈0.77, 1.04, and 1.2 molecules/nm^2, respectively; it was assumed that the molecular extinction coefficients (ε) of the films are similar to those observed in acetonitrile solution for the MLCT band, viz. $\varepsilon \approx$ 23 000, 29 770, and 27 450 cm^{-1} M^{-1} at λ_{max} = 569, 490 and 490 nm for Fe-PT, Ru-PT, and Os-PT, respectively. These data imply a certain reactivity trend of the M-PT complexes (for quaternization reaction) with the functionalized substrate (from the same batch) in following order Os-PT > Ru-PT > Fe-PT, even though it is not clear at the moment whether this trend can be considered as fully reliable. The full width at half maximum (FWHM) for the MLCT band of the Fe-PT, Ru-PT and Os-PT template layers on glass was found to be 60, 67, and 56 nm, respectively, which is higher by 18, 14, and 9 nm, respectively, than the values obtained for Fe-PT, Ru-PT, and Os-PT in acetonitrile solution. The above broadening of the MLCT band might be related to the intermolecular interaction, i.e., chromophore-to-chromophore charge transfer which is hardly possible in solution but can occur in densely packed molecular films on solid substrates.[3e,17] Further, the separation between the valence and conduction bands, i.e., the optical band gap (E_g) for the Fe-PT, Ru-PT and Os-PT template layers on glass substrates was estimated by extrapolating the MLCT band[18] and found at E_g = 1.84, 2.04, and 1.64 eV, respectively. These values are comparable to the optical band gap of Fe-PT, Ru-PT and Os-PT in CH_3CN solution which is only slightly lower (by 0.12, 0.2, and 0.02 eV, respectively).

Remarkably, coordination of copper ion with the secondary template layers (M-PT) shows no significant change in the UV-Vis spectra except a very slight increase in intensity (Figure 4), which means that the linker does not disturb the optical properties of the M-PT layers. At the same time, a combination of two different M-PT moieties as a molecular dyad results in a joint spectrum, which exhibits the characteristic MLCT bands of both components. In particular, the spectrum of the Fe-PT/Cu/Ru-PT monolayer on glass in Figure 4a shows a new, Ru-PT-related band at λ_{max} = 502 nm in addition to the band of the Fe-PT/Cu template layer, which evidences the dyad formation and manifests an extension of the optical window of the system into the visible region (λ = 400–700 nm). In addition, the original MLCT band of the Fe-PT template layer at λ = 605 nm was blue shifted (–6 nm), slightly broadened (≈12 nm), and exhibits little higher absorptivity (Figure 4a). This behavior indicates an intramolecular electronic communication between the Fe-PT and Ru-PT units connected via the Cu linker. Similarly, the UV-Vis spectrum of the Ru-PT/Cu/Os-PT film in Figure 4b exhibits a new, Os-PT-related band at λ = 687 nm in addition to the band of Ru-PT which shifts to ≈502 nm as compared to the Ru-PT template layer (≈511 nm), along with some broadening ($\Delta\lambda$ = 30 nm) and increase in intensity (by a factor of ≈1.7). These data confirm the dyad formation. Note that the broad and intense band, observed at λ_{max} = 502 nm, stems from the merge of the MLCT bands of Ru-PT and Os-PT which are quite close to one another. Finally, the UV-vis spectrum of the Os-PT/Cu/Fe-PT film in Figure 4c shows a new, Fe-PT related band at λ = 577 nm in addition to the bands of Os-PT, manifesting the formation of the dyads. The resulting three bands (^{1}MLCT, ^{3}MLCT and ^{3}MLCT) cover the entire visible region. Also in this case, the Fe-PT band was blue shifted (–25 nm) and broadened as compared to the Fe-PT/Cu template layer, which indicates a strong, Cu-mediated communication between the Os-PT and Fe-PT units.

A course estimate for the coupling efficiency of the second M-PT unit to the M-PT/Cu template was obtained by subtraction of the spectrum of the Cu-terminated template layer from that of the molecular dyad. The density of Ru-PT, Os-PT, and Fe-PT in the Fe-PT/Cu/Ru-PT, Ru-PT/Cu/Os-PT and Os-PT/Cu/Fe-PT monolayers was estimated at 0.67, 0.98, and 0.90 molecules/nm^2, respectively. This corresponds to a coupling efficiency of ≈87%, ≈94%, and ≈75% for the Fe-PT/Cu/Ru-PT, Ru-PT/Cu/Os-PT and Os-PT/Cu/Fe-PT dyad films, respectively. Remarkably, these data represent similar reactivity trend of M-PT (i.e., Os-PT > Ru-PT > Fe-PT) with Cu-terminated template layers (coordination reaction), as was observed (vide supra) with the iodo-terminated template layers (quaternization reaction). Further, E_g of the dyad assemblies were found to be somewhat lower than the analogous values for the respective

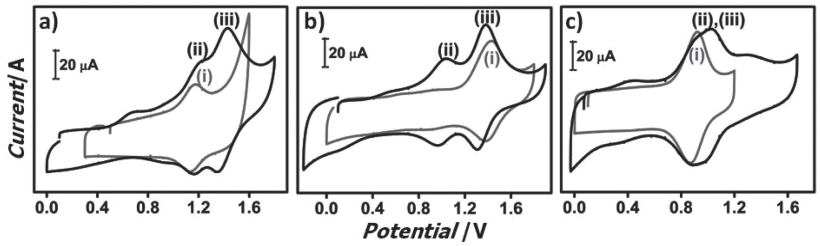

Figure 5. Cyclic voltammograms of the secondary template layers (gray lines) and hetero-metallic molecular dyads (black lines) on ITO-coated glass substrates. a) Fe-PT template layer and Fe-PT/Cu/Ru-PT dyad layer: i) Fe^{II}/Fe^{III}, ii) Fe^{II}/Fe^{III} and iii) Ru^{II}/Ru^{III}. b) Ru-PT template layer and Ru-PT/Cu/Os-PT dyad layer: i) Ru^{II}/Ru^{III}, ii) Os^{II}/Os^{III} and iii) Ru^{II}/Ru^{III}. c) Os-PT template layer and Os-PT/Cu/Fe-PT dyad layer: i) Os^{II}/Os^{III}, ii) Fe^{II}/Fe^{III} and iii) Os^{II}/Os^{III}.

template layer. For instance, the optical band gap for the Fe-PT/Cu/Ru-PT, Ru-PT/Cu/Os-Pt and Os-PT/Cu/Fe-PT dyad assemblies was estimated at E_g = 1.79, 1.67, and 1.61 eV, respectively, which are lower than the E_g values for the Fe-PT, Ru-PT and Os-PT template layers (vide supra). These findings suggest enhanced electronic conductivity of the dyads assemblies as compared to the template layers.

2.4. Electrochemical Properties

The electrochemical behavior of the template layers and hetero-metallic molecular dyads was investigated using cyclic voltammetry and the results of these experiments are presented in **Figure 5**. A reversible one-electron redox process due to $M^{II/III}$ (M = Fe, Ru, or Os) was observed for all the template layers (M-PT). The shape and behavior of the signal exhibit typical characteristics of surface bound species.[19] The half-wave redox potentials, $E_{1/2}$ for the Fe-PT, Ru-PT, and Os-PT template layers were found to be +1.18, +1.40, and +0.89 V (vs. Ag/AgCl), respectively. Large differences between the positions of the redox peaks of these redox-active template layers suggest that the related hetero-metallic molecular dyads can be a viable system for multiple charge storage. Notably, the difference between the $E_{1/2}$ values for Fe-PT and Ru-PT was +0.19 in CH_3CN solution (see Figure S4, Supporting Information) but became higher (+0.22) for the respective template layers. The peak-to-peak separation, ΔE_P, between the anodic and cathodic waves for all the template layers was found to be in a range of ≈30–40 mV at 0.1 V/s; it increases linearly with increasing scan rate, reaching 40–55 mV at a scan rate of 1.0 V/s. This behavior is probably related to iR-drop and/or to the influence of heterogeneous electron transfer kinetics.[7a,20] The FWHM of the oxidation peak ($\Delta E_{P,1/2}$) was found to be 120–140, 190–210, and 150–205 mV for the Fe-PT, Ru-PT and Os-PT template layers, respectively, which deviate from the value typical of the ideal Nernstian electrochemical reactions ($\Delta E_{P,1/2}$ = 90 mV), indicating the redox site–site interactions and/or site heterogeneity.[7a,21] The surface coverage, Γ_S was estimated from the peak current density (I_{pc}, I_{pa}), assuming that all molecules get oxidized or reduced, and found to be 0.64, 1.3, and 1.5 molecules/nm^2 for the Fe-PT, Ru-PT and Os-PT template layers, respectively, which is in reasonable agreement with the analogous values obtained from the UV-Vis data for the case of ITO-coated glass substrates, viz. 0.76, 1.35, and 1.46 molecules/nm^2. These data suggest that a reasonable amount of charge (75–150 × 10^{12} electrons/cm^2) can be stored using the Fe-PT, Ru-PT and Os-PT template layers. A linear correlation (R^2 = 0.98–0.99) between the peak current I_p (both cathodic and anodic) and the scan rate (see Figure S5, Supporting Information) for all the template layers suggests that the redox process at the solid-liquid interface is not controlled by diffusion of molecules. The I_{pa}/I_{pc} ratio is almost independent of the scan rate and close to one for all template layers (see Figure S6, Supporting Information) indicating high stability and reversibility of both redox states. Attempts were made to scan the reduction waves at a negative potential that resulted in dissolution of the template layers at voltages below −1.2 V.

Notably, the presence of reversible redox states (oxidized and reduced) in the template layers is highly advantageous for writing and erasing the information in the form of charge while applying particular potentials. For instance, application of an oxidizing potential (1.17, 1.42 or 0.92 V for the Fe-PT, Ru-PT and Os-PT template layers, respectively) should cause the transfer of an electron from the immobilized molecules to the substrate, resulting in storage of positive charge, whereas application of a reducing potential (1.13, 1.39 or 0.88 V for the Fe-PT, Ru-PT and Os-PT template layers, respectively) should cause the transfer of an electron back to the molecules, thus reconfiguring the stored charge. Notably, this read-write process have been carried out for 10^3 cycles (see Figure S7a, Supporting Information) and the data show minimal variation (<10%), which indicates that the system is robust and the charge is delocalized throughout the molecule, i.e., over the entire conjugated ligand system, thereby reducing the number of "hot spots" and protected from the adventitious chemical reagents such as electrolytes ($^tBuNPF_6$), solvent (CH_3CN) or internal reference electrode (ferrocene) over large number of read-write cycles.

Cyclic voltammetry experiments for the dyads also exhibit distinct reversible redox peaks attributed to the $Fe^{II/III}$, $Ru^{II/III}$ or $Os^{II/III}$ centers (vide infra). In particular, cyclic voltammogram of the Fe-PT/Cu/Ru-PT monolayer in Figure 5a exhibits two distinct redox peaks due to the Fe^{II}/Fe^{III} and Ru^{II}/Ru^{III} couples. The half-wave redox potential, $E_{1/2}$ associated with the Fe^{II}/Fe^{III} couple was observed at +1.19 V, whereas for Ru^{II}/Ru^{III} it was found at +1.41 V (vs. Ag/AgCl). Remarkably, the $E_{1/2}$ value related to Fe^{II}/Fe^{III} in the Fe-PT/Cu/Ru-PT film was observed at a higher potential (+0.04 V) than the corresponding value for the Fe-PT-template layer, whereas the $E_{1/2}$ related to Ru^{II}/Ru^{III} was observed at a lower potential (−0.01 V) than the corresponding Ru-PT template layer. This observation indicates transfer of electron density within the dyad from the Fe to Ru center via the Cu linker. As a result, oxidation of the Ru center requires a lower potential. Apparently, the ratio of anodic to cathodic peak currents (I_{pa}/I_{pc}) is close to one for the surface-confined reversible redox species (see Figure S5, Supporting Information).

Cyclic voltammogram of the Ru-PT/Cu/Os-PT monolayer is presented in Figure 5b. We observe a sharper redox peak of

the Ru center as compared to that of the Os center. The $E_{1/2}$ value of the Os center in the Ru-PT/Cu/Os-PT film (+1.0 V, vs. Ag/AgCl) is higher by 0.11 V than that for the Os-PT template film (Figure 5b), whereas $E_{1/2}$ for the Ru center (+1.35 V, vs. Ag/AgCl) is lower by 0.05 V than that for the Ru-PT template film, which indicates a transfer of electron density from the Os to Ru center. Remarkably, the extent of this transfer is higher than that from the Fe to Ru center in the case of the Fe-PT/Cu/Ru-PT assembly.

Interestingly, in the case of the Os-PT/Cu/Fe-PT monolayer, the peaks associated with the Fe and Os centers merge together and give a single broad peak that might be useful for storing more bits of one kind of information. The half-wave potential, $E_{1/2}$ was estimated at +0.97 V (vs. Ag/AgCl). Note that the electrolyte solution was cross-checked optically (UV-Vis) as well as electrochemically after the above electrochemical experiments and no signal was observed indicating that desorption of molecules from the substrate did not occur. Note also that the redox potentials for the individual molecular dyads depend on electron donating or withdrawing effect of one substituent on other. The strong peaks observed for both components of the dyads indicate that the film structure is porous enough to allow the penetration of electrolytes to the underlying ITO substrate.[22] Moreover, the system exhibited excellent redox reversibility (see Figure S7b, Supporting Information) and displayed minimum degradation (<10%) after 10^3 oxidation/reduction cycles.

Note that presence of distinct redox states in molecular dyads is equivalent to the change of a bit information from "0" to "1". For instance, the presence of two distinct cationic redox states gives rise to three states of memory ("00", "10" and "11"). The "00" memory state corresponds to the neutral state of both components (nonoxidized, at 0 V or above), "10" memory state corresponds to the oxidation of one component at the respective lower oxidation potential and "11" memory state corresponds to the oxidation of both components at the respective higher oxidation potential. Reduction potential corresponds to subsequent erasing the stored charge and return to the initial state. Notably, the charge-retention time of the system can be tuned by inserting a barrier between the redox center/centers and the substrate.[23] In the given case, the presence of the short aliphatic coupling layer increases the charge-retention time and thereby creates a current gap between the oxidized and reduced species in the system.

3. Conclusions

Monomolecular films of redox-active, surface-confined heterometallic molecular dyads (SURHMDs) were fabricated on Si(100), glass, and ITO-coated glass substrates and characterized by a variety of complementary surface analysis techniques including AFM, XPS, and NEXAFS spectroscopy. These dyads combine two different Fe-, Ru- and Os-based polypyridyl complexes bridged by a Cu ion linker. The UV-Vis spectra of the dyad films represent a superposition of the spectra of their both building blocks, exhibiting characteristic bands of the individual complexes. As a result, the optical windows of the dyad films cover the entire visible region (λ = 400–800 nm), which is of importance for potential applications.[24] Beyond favorable optical properties, the dyad monolayers exhibit useful electrochemical behavior, showing, in particular, multiple and well distinguishable redox potentials owing to the cross combinations of the Fe, Ru, and Os based complexes. In addition, the dyad films exhibit Cu-mediated intramolecular charge transfer between the individual metal centers.

The above monomolecular assemblies of the molecular dyads open a new avenue for applications of these and similar systems in molecular-based electronic devices for charge storage and transfer, as well as for memory, and logic operations.[8,25] Interestingly, the presence of the multiple redox sites provides multiple information storage capability, whereas the merged redox site (broad peak for Os-PT/Cu/Fe-PT) offers a larger bit (size) for storing one kind of information. We believe that the high electrochemical stability and reusability of the dyad monolayers can make them potential alternatives to the existing semiconductor-based memory devices such as dynamic random access memory, DRAM, and FLASH memory.[26]

The suggested surface-supported stepwise coordination reaction methodology is attractive, synthetically feasible, and relatively simple as compared to a synthesis of a single molecule that exhibits multiple redox states or to preparation of a mixed SAM that probably bounces non-identical ratio of each component due to dissimilar adsorption activity. In addition, the suggested approach should be well suitable to extend the system to triad, tetrad etc. in order to increase the number of redox states or stored bits. Moreover, the terminal pyridine moiety can serve as a donor for other metals (e.g., Pd or Ag) to confine nanoparticles or can be capped simply by using acid.[27]

4. Experimental Section

Formation of Template Layers: The freshly cleaned glass, ITO-coated glass and Si substrates (25 mm × 10 mm × 1 mm) were functionalized with 3-iodo-*n*-propyltrimethoxy-silane under N_2 atmosphere using Schlenk line.[28] For instance, the substrates were treated with a dry *n*-pentane solution of 3-iodo-*n*-propyltrimethoxy-silane (200:1) at room temperature for 30 min under N_2 atmosphere. Then the substrates were thoroughly washed with dry *n*-pentane and sonicated (for 3 min each) with *n*-pentane, followed by dichloromethane (DCM) and 2-propanol to remove any physisorbed materials. The resulting films were dried properly under a stream of N_2 followed by drying in oven at 120 °C for 15 min. Consequently, the functionalized substrates were placed into 50 mL Teflon-lined autoclave and immersed in dry acetonitrile/toluene (1:1, v/v) solution of complexes (0.5 mM), then kept at 85 °C for 60h in a programmed oven. It was cooled to room temperature. The functionalized substrates were then rinsed with acetonitrile and sonicated for 3 min each in acetonitrile, acetone and 2-propanol to remove the physisorbed materials. Finally, the samples were carefully wiped with a wet task wipe and dried under a stream of N_2.

Fabrication of Heterometallic Molecular Dyads: The formation of molecular dyads was monitored by UV-vis and cyclic voltammetry. After recording the UV-vis spectra of the template layer, the substrates were immersed in 0.5 mM solution of $Cu(NO_3)_2$ in acetonitrile for 30 min at room temperature under dark conditions. The samples were then washed in acetonitrile, dried under a stream of N_2, and subjected to the UV-Vis characterization. Subsequently, the samples were immersed in a 0.5 mM solution of dissimilar metallo-ligand in acetonitrile for 30 min at room temperature under dark conditions. Notably, increasing of immersion time (≈1 h) did not affect the intensity of UV-Vis spectra. The samples were then washed in acetonitrile followed by drying under N_2 stream.

Characterization of the SURHMD Monolayers: Atomic force microscopy (AFM) images were recorded on silicon substrates using a Dimension 3100 (Veeco Digital Instruments) device equipped with a Nanoscope IIIa controller (Veeco) and operating in tapping/semicontact mode in air. For these experiments, we used aluminium-coated cantilevers with silicon nitride tips having a radius of less than 10 nm. The thickness measurements were carried out using J. A. Woollam model M-2000 V spectroscopic ellipsometer in 400–800 nm range with VASE32 software. Parameters A, B and C were 1.4, 0.02, and 0.01 respectively, with MSE < 10 for a Cauchy model. The SiO_2 layer was calibrated to be 15 Å. Wettability of the samples was measured with a Rame-Hart goniometer using double distilled water drops.

Spectroscopic monitoring of the SURHMDs preparation process and characterization of the resulting SURHMDs was performed by means of XPS and NEXAFS spectroscopy. The experiments were carried out under room temperature and ultrahigh vacuum (UHV) conditions with a base pressure of at least 1.5×10^{-9} mbar or higher. The time for the acquisition of the spectra was carefully selected to avoid any noticeable damage of the samples by the primary X-rays.[29]

XPS measurements were performed both with a laboratory spectrometer and at the bending magnet HE-SGM beamline at the synchrotron storage ring BESSY II in Berlin (Germany). The spectra were recorded in normal emission geometry. The binding energy scale of XPS spectra was referenced to the Si $2p_{3/2,\ 1/2}$ doublet at 99.15 eV.[30] The energy resolution was ≈0.9 eV for the laboratory spectrometer and ≈0.3 eV at the synchrotron.

The NEXAFS spectra were acquired at C and N K-edges in the partial electron yield mode with retarding voltages of −150 V and −300 eV, respectively, and linearly polarized light with a polarization factor of ≈91%. To gain information about the orientational order in the molecular films the geometry of the primary X-ray was varied from normal to grazing incidence in steps of 10–20°. The energy resolution of the NEXAFS spectra was about 0.3 eV. The raw spectra were normalized by dividing by the incident photon flux for a clean gold reference sample and the energy scale was calibrated to the most pronounced π* resonance of highly oriented pyrolytic graphite at 285.38 eV.[31]

UV-Vis Experiments: UV-vis spectra were recorded at room temperature with a JASCO (Model No. V-670) spectrophotometer in transmission mode (200–800 nm). The functionalized glass substrates were fixed in a Teflon holder (1.5 cm × 0.75 cm window) and an identical bare glass substrate without monolayer was used to compensate for the background absorption.

Electrochemical Experiments: The electrochemical experiments were performed with a CH Instruments potentiostat (Model 660D). Cyclic voltammograms were measured on 1 mM solutions of the complexes in dry acetonitrile with tetra-*n*-butylammoniumhexafluoro-phosphate ($TBAPF_6$, 0.1 M) as the supporting electrolyte using a glassy carbon as working electrode, a Pt wire as counter electrode, and Ag/AgCl as a reference electrode. In the case of the surface based electrochemistry, ITO-coated glass was used as working electrode (WE), Pt-wire as counter electrode (CE), and Ag/AgCl as reference electrode. $TBAPF_6$ (20 mM) in acetonitrile was used as supporting electrolyte.

Supporting Information

Supporting Information is available from the Wiley Online Library or from the author.

Acknowledgements

This research was supported by the Department of Science and Technology, Nano-Mission (SR/NM/NS-12/2010), University of Delhi, Delhi, and the German Research Society, (DFG projects ZH 63/9-3 and ZH 63/14-1). T.G. thanks the Alexander von Humboldt (AvH) foundation for a Humboldt fellowship of experience researcher. P.C.M. thanks the Council of Scientific and Industrial Research for a junior research fellowship. M.Z. and J.Y.L. thank A. Nefedov and Ch. Wöll (KIT) for the technical cooperation at BESSY II as well as BESSY II staff for the assistance during the synchrotron-based experiments.

Received: November 20, 2012
Revised: February 4, 2013
Published online: March 27, 2013

[1] a) N. Miyashita, D. G. Kurth, *J. Mater. Chem.* **2008**, *18*, 2636; b) P. C. Mondal, B. Gera, T. Gupta, *Advanced Organic-Inorganic Composites: Materials Device and Allied Applications*, Nova Science Publishers, Inc., New York **2012**, p. 33; c) H. C. Streit, M. Adlung, O. Shekhah, X. Stammer, H. K. Arslan, O. Zybaylo, T. Ladnorg, H. Gliemann, M. Franzreb, C. Woell, C. Wickleder, *ChemPhysChem* **2012**, *13*, 2699; d) O. Shekhah, J. Liu, R. A. Fischer, C. Woell, *Chem. Soc. Rev.* **2011**, *40*, 1081; e) N. Lin, S. Stepanow, M. Ruben, J. V. Barth, *Top. Curr. Chem.* **2009**, *287*, 1; f) R. J. Forster, T. E. Keyes, *Coord. Chem. Rev.* **2009**, *253*, 1833; g) F. Cattaruzza, A. Llanes-Pallas, A. G. Marrani, E. A. Dalchiele, F. Decker, R. Zanoni, M. Prato, D. Bonifazi, *J. Mater. Chem.* **2008**, *18*, 1570.

[2] a) J. S. Lindsey, D. F. Bocian, *Acc. Chem. Res.* **2011**, *44*, 638; b) B. Fabre, *Acc. Chem. Res.* **2010**, *43*, 1509; c) Z. Liu, A. A. Yasseri, J. S. Lindsey, D. F. Bocian, *Science* **2003**, *302*, 1543; d) T. Gupta, M. E. van der Boom, *Angew. Chem. Int. Ed.* **2008**, *47*, 2260.

[3] a) P. C. Mondal, J. Y. Lakshmanan, H. Hamoudi, M. Zharnikov, T. Gupta, *J. Phys. Chem. C* **2011**, *115*, 16398; b) R. Kaminker, L. Motiei, A. Gulino, I. Fragala, L. J. W. Shimon, G. Evmenenko, P. Dutta, M. A. Iron, M. E. van der Boom, *J. Am. Chem. Soc.* **2010**, *132*, 14554; c) L. Motiei, M. Altman, T. Gupta, F. Lupo, A. Gulino, G. Evmenenko, P. Dutta, M. E. van der Boom, *J. Am. Chem. Soc.* **2008**, *130*, 8913; d) M. Altman, A. D. Shukla, T. Zubkov, G. Evmenenko, P. Dutta, M. E. van der Boom, *J. Am. Chem. Soc.* **2006**, *128*, 7374; e) T. Gupta, M. Altman, A. D. Shukla, D. Freeman, G. Leitus, M. E. Van der Boom, *Chem. Mater.* **2006**, *18*, 1379; f) J. F. Jinliang Zhuang, Andreas Terfort, *Beilstein J. Nanotechnol.* **2012**, *3*, 570; g) C. Carbonell, I. Imaz, D. Maspoch, *J. Am. Chem. Soc.* **2011**, *133*, 2144; h) E. Bellido, S. Cardona-Serra, E. Coronado, D. Ruiz-Molina, *Chem. Commun.* **2011**, *47*, 5175; i) B. Liu, M. Ma, D. Zacher, A. Betard, K. Yusenko, N. Metzler-Nolte, C. Woll, R. A. Fischer, *J. Am. Chem. Soc.* **2011**, *133*, **1734**.

[4] a) K. M. Roth, N. Dontha, R. B. Dabke, D. T. Gryko, C. Clausen, J. S. Lindsey, D. F. Bocian, W. G. Kuhr, *J. Vac. Sci. Technol., B* **2000**, *18*, 2359; b) K. M. Roth, J. S. Lindsey, D. F. Bocian, W. G. Kuhr, *Langmuir* **2002**, *18*, 4030; c) Q. Li, G. Mathur, S. Gowda, S. Surthi, Q. Zhao, L. Yu, J. S. Lindsey, D. F. Bocian, V. Misra, *Adv. Mater.* **2004**, *16*, 133; d) J. Jiao, E. Nordlund, J. S. Lindsey, D. F. Bocian, *J. Phys. Chem. C* **2008**, *112*, 6173; e) I. Schmidt, J. Jiao, P. Thamyongkit, D. S. Sharada, D. F. Bocian, J. S. Lindsey, *J. Org. Chem.* **2006**, *71*, 3033.

[5] a) E. C. Constable, *Chem. Soc. Rev.* **2007**, *36*, 246; b) T. Gupta, M. E. Van der Boom, *J. Am. Chem. Soc.* **2006**, *128*, 8400; c) A. D. Shukla, A. Das, M. E. van der Boom, *Angew. Chem. Int. Ed.* **2005**, *44*, 3237; d) F. A. Murphy, S. Suarez, E. Figgemeier, E. R. Schofield, S. M. Draper, *Chem. Eur. J.* **2009**, *15*, 5740; e) V. Balzani, A. Juris, M. Venturi, S. Campagna, S. Serroni, *Chem. Rev.* **1996**, *96*, 759; f) Y. Nishimori, K. Kanaizuka, T. Kurita, T. Nagatsu, Y. Segawa, F. Toshimitsu, S. Muratsugu, M. Utsuno, S. Kume, M. Murata, H. Nishihara, *Chem. Asian J.* **2009**, *4*, 1361.

[6] a) H. Maeda, R. Sakamoto, Y. Nishimori, J. Sendo, F. Toshimitsu, Y. Yamanoi, H. Nishihara, *Chem. Commun.* **2011**, *47*, 8644; b) G. Tsekouras, O. Johansson, R. Lomoth, *Chem. Commun.* **2009**, 3425; c) M. J. J. P. Silva, P. Bertoncello, N. N. Daskalakis, N. Spencer, B. M. Kariuki, P. R. Unwin, Z. Pikramenou, *Supramol. Chem.* **2007**, *19*, 115; d) Y. Nishimori, K. Kanaizuka, M. Murata,

H. Nishihara, *Chem. Asian J.* **2007**, *2*, 367; e) H. Nishihara, K. Kanaizuka, Y. Nishimori, Y. Yamanoi, *Coord. Chem. Rev.* **2007**, *251*, 2674; f) M.-a. Haga, T. Takasugi, A. Tomie, M. Ishizuya, T. Yamada, M. D. Hossain, M. Inoue, *Dalton Trans.* **2003**, 2069.

[7] a) E. Figgemeier, E. C. Constable, C. E. Housecroft, Y. C. Zimmermann, *Langmuir* **2004**, *20*, 9242; b) R. J. Forster, T. E. Keyes, *J. Phys. Chem. B* **2001**, *105*, 8829.

[8] a) T. Kurita, Y. Nishimori, F. Toshimitsu, S. Muratsugu, S. Kume, H. Nishihara, *J. Am. Chem. Soc.* **2010**, *132*, 4524; b) H. Wolpher, S. Sinha, J. Pan, A. Johansson, M. J. Lundqvist, P. Persson, R. Lomoth, J. Bergquist, L. Sun, V. Sundstroem, B. Akermark, T. Polivka, *Inorg. Chem.* **2007**, *46*, 638.

[9] E. C. Constable, A. M. W. C. Thompson, *J. Chem. Soc., Dalton Trans.* **1994**, 1409.

[10] N. Gauthier, G. Argouarch, F. Paul, M. G. Humphrey, L. Toupet, S. Ababou-Girard, H. Sabbah, P. Hapiot, B. Fabre, *Adv. Mater.* **2008**, *20*, 1952.

[11] E. C. Constable, E. Figgemeier, C. E. Housecroft, J. Olsson, Y. C. Zimmermann, *Dalton Trans.* **2004**, 1918.

[12] J. E. Beves, E. C. Constable, C. E. Housecroft, M. Neuburger, S. Schaffner, *CrystEngComm* **2008**, *10*, 344.

[13] Y. Zubavichus, M. Zharnikov, Y. Yang, O. Fuchs, E. Umbach, C. Heske, A. Ulman, M. Grunze, *Langmuir* **2004**, *20*, 11022.

[14] J. Stöhr, *NEXAFS Spectroscopy: Springer Series in Surface Science 25*, Springer-Verlag, Berlin **1992**.

[15] a) J. A. Horsley, J. Stohr, A. P. Hitchcock, D. C. Newbury, A. L. Johnson, F. Sette, *J. Chem. Phys.* **1985**, *83*, 6099; b) C. Kolczewski, R. Puttner, O. Plashkevych, H. Agren, V. Staemmler, M. Martins, G. Snell, A. S. Schlachter, M. Sant'Anna, G. Kaindl, L. G. M. Pettersson, *J. Chem. Phys.* **2001**, *115*, 6426.

[16] A. D. Shukla, D. Strawser, A. C. B. Lucassen, D. Freeman, H. Cohen, D. A. Jose, A. Das, G. Evmenenko, P. Dutta, M. E. Van der Boom, *J. Phys. Chem. B* **2004**, *108*, 17505.

[17] a) K. öberg, U. Edlund, B. Eliasson, A. Shchukarev, K. Seshadri, D. Allara, *J. Phys. Chem. B* **2000**, *104*, 10627; b) S-H. Hsu, D. N. Reinhoudt, J. Huskens, A. H. Velders, *J. Mater. Chem.* **2011**, *21*, 2428; c) L. de Leon, M. C. Biewer, *Tetrahedron Lett.* **2000**, *41*, 3527.

[18] a) J. Eldo, A. Ajyaghosh, *Chem. Mater.* **2002**, *14*, 410; b) E. Bundgaard, F. C. Krebs, *Macromolecules* **2006**, *39*, 2823.

[19] T. Gupta, R. Cohen, G. Evmenenko, P. Dutta, M. E. Van der Boom, *J. Phys. Chem. C* **2007**, *111*, 4655.

[20] a) D. A. Walsh, T. E. Keyes, R. J. Forster, *J. Phys. Chem. B* **2004**, *108*, 2631; b) A. J. Bard, L. R. Faulkner, *Electrochemical Methods: Fundamentals and Applications*; 2nd ed, John Wiley & Sons, New York **2001**; c) Q. Li, S. Surthi, G. Mathur, S. Gowda, V. Misra, T. A. Sorenson, R. C. Tenent, W. G. Kuhr, S.-i. Tamaru, J. S. Lindsey, Z. Liu, D. F. Bocian, *Appl. Phys. Lett.* **2003**, *83*, 198; d) K. M. Roth, A. A. Yasseri, Z. Liu, R. B. Dabke, V. Malinovskii, K.-H. Schweikart, L. Yu, H. Tiznado, F. Zaera, J. S. Lindsey, W. G. Kuhr, D. F. Bocian, *J. Am. Chem. Soc.* **2003**, *125*, 505.

[21] P. Delahay, *Double Layer and Electrode Kinetics*; Interscience, New York **1965**.

[22] L. Motiei, R. Kaminker, M. Sassi, M. E. van der Boom, *J. Am. Chem. Soc.* **2011**, *133*, 14264.

[23] M. Sierra, M. A. Herranz, S. Zhang, L. Sanchez, N. Martin, L. Echegoyen, *Langmuir* **2006**, *22*, 10619.

[24] a) T. Gupta, A. Kumar, *Analyst* **2011**, *136*, 4127; b) T. Gupta, E. Tartakovsky, M. A. Iron, M. E. van der Boom, *ACS Appl. Mater. Interfaces* **2010**, *2*, 7; c) J. R. Durrant, S. A. Haque, E. Palomares, *Chem. Commun.* **2006**, 3279.

[25] a) K. Terada, K. Kanaizuka, V. M. Iyer, M. Sannodo, S. Saito, K. Kobayashi, M.-a. Haga, *Angew. Chem. Int. Ed.* **2011**, *50*, 6287; b) T. Gupta, M. E. van der Boom, *Angew. Chem. Int. Ed.* **2008**, *47*, 5322; c) G. de Ruiter, M. E. van der Boom, *Acc. Chem. Res.* **2011**, *44*, 563; d) G. de Ruiter, M. E. van der Boom, *Angew. Chem. Int. Ed.* **2012**, *51*, 8598.

[26] A. N. Shipway, E. Katz, I. Willner, *Struct. Bonding* **2001**, *99*, 237.

[27] a) C. Silien, D. Lahaye, M. Caffio, R. Schaub, N. R. Champness, M. Buck, *Langmuir* **2011**, *27*, 2567; b) C. Silien, M. Buck, G. Goretzki, D. Lahaye, N. R. Champness, T. Weidner, M. Zharnikov, *Langmuir* **2009**, *25*, 959.

[28] a) C. Haensch, S. Hoeppener, U. S. Schubert, *Chem. Soc. Rev.* **2010**, *39*, 2323; b) R. Sfez, D.-Z. Liu, I. Turyan, D. Mandler, S. Yitzchaik, *Langmuir* **2001**, *17*, 2556; c) H. G. Hong, M. Jiang, S. G. Sligar, P. W. Bohn, *Langmuir* **1994**, *10*, 153.

[29] a) K. Heister, M. Zharnikov, M. Grunze, L. S. O. Johansson, A. Ulman, *Langmuir* **2001**, *17*, 8; b) M. Zharnikov, *J. Electron Spectrosc. Relat. Phenom.* **2010**, *178–179*, 380.

[30] J. F. Moulder, W. E. Stickle, P. E. Sobol, K. D. Bomen, *Handbook of X-ray Photoelectron Spectroscopy*, Perkin-Elmer Corp., Eden Prairie, MN **1992**.

[31] P. E. Batson, *Phys. Rev. B Condens. Matter* **1993**, *48*, 2608.